2 Nonlinear Optical Techniques for Terahertz Pulse Generation and Detection—Optical Rectification and Electrooptic Sampling

Ingrid Wilke and Suranjana Sengupta
Rensselaer Polytechnic Institute

CONTENTS

2.1 INTRODUCTION

The generation and detection of short pulses of terahertz (THz) frequency electromagnetic radiation are attracting great interest. Research activities in this area are driven by applications of THz-frequency radiation pulses in time-domain THz spectroscopy and time-domain THz imaging.[1,2] Recent examples of major scientific advancements in THz wave research include the detection of single-base pair differences in femtomolar concentrations of DNA,[3] the observation of the temporal evolution of exciton formation in semiconductors[4] and understanding of carrier dynamics in high-temperature superconductors.[5] Real-world applications of time-domain THz spectroscopy and imaging address important problems such as nondestructive testing,[6] as well as new approaches to medical diagnostics and rapid screening in drug development.[7]

One of the research directions in THz science and technology is to increase the bandwidth of short THz-frequency radiation pulses. Nonlinear optical phenomena such as optical rectification and the linear electrooptic effect (Pockels' effect) are attractive options for broadband generation and detection of THz radiation.

This chapter provides an overview of the generation and detection of freely propagating THz pulses based on nonlinear optical techniques. In Section 2.1.1 of this chapter, the principles of time-domain THz spectroscopy and time-domain THz imaging using nonlinear optical techniques for THz pulse generation and detection are briefly discussed. Section 2.2 describes the principles of generation and detection of THz-frequency radiation by optical rectification of femtosecond laser pulses and femtosecond electrooptic sampling. THz radiation emission has been reported from a variety of nonlinear materials such as lithium niobate ($LiNbO_3$),[8,9] lithium tantalate ($LiTaO_3$),[9,10] zinc telluride (ZnTe),[11,12] indium phosphide (InP),[13] gallium arsenide (GaAs),[14] gallium selenide (GaSe),[15,16] cadmium telluride (CdTe),[17] cadmium zinc telluride (CdZnTe),[18] DAST,[10,19] and metals.[20,21] Section 2.3 summarizes the performance of THz emitters based on these materials in terms of bandwidth and signal strength of the emitted THz radiation. Materials for the detection of THz radiation by femtosecond electrooptic sampling are the subjects of Section 2.4. In Section 2.5, an application of electrooptic detection of THz-frequency electromagnetic transients is discussed.

2.1.1 Terahertz Time-Domain Spectroscopy: An Overview

The basic ideas of time-domain THz spectroscopy and a time-domain THz imaging system is illustrated in Figure 2.1. A subpicosecond pulse of THz-frequency electromagnetic radiation passes through a sample placed in the THz beam and its time profile is compared to a reference pulse. The latter can be a freely propagating pulse or a pulse propagating through a medium with known properties. The frequency spectra of the transmitted and reference THz radiation pulses are obtained by Fourier transformation. Analysis of the frequency spectra yields spectroscopic information on the material under investigation. In the case of time-domain THz imaging the THz radiation focal spot is scanned across the sample and a THz image of the object under investigation is obtained.

The time-domain THz spectroscopy system shown in Figure 2.1 is powered by a laser, which emits a train of femtosecond duration pulses at near-infrared frequencies.

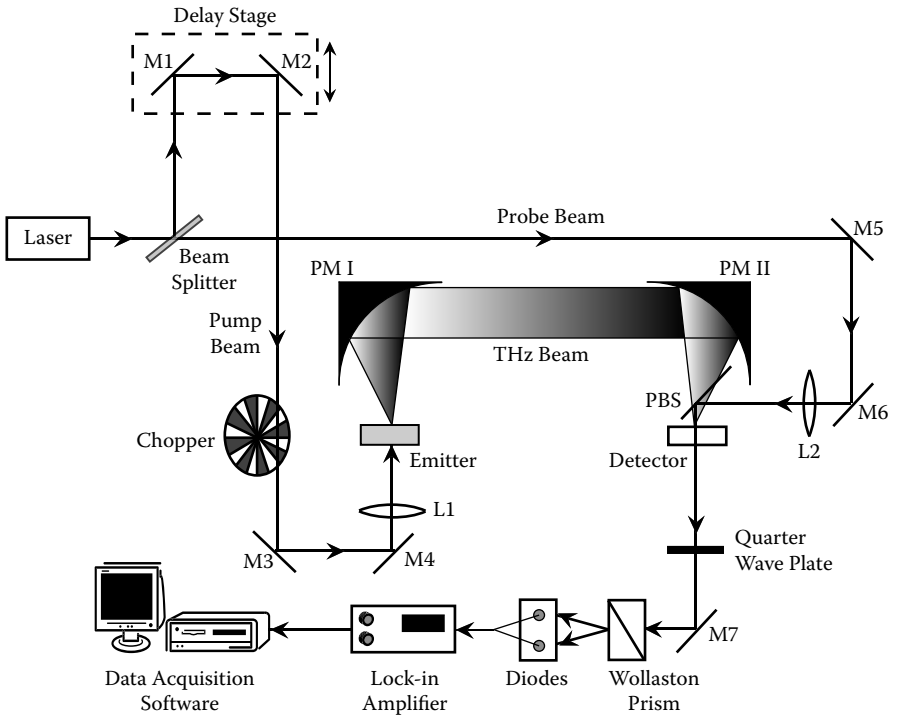

FIGURE 2.1 Experimental arrangements for time-domain THz spectroscopy measurements using nonlinear optical techniques for the generation and detection of freely propagating THz-radiation pulses. (M1–M7 optical beam steering mirrors, PMI, PMII parabolical THz-beam steering mirrors, L1, L2 lenses).

The initial laser beam after passing through a beam splitter is split into two parts: the pump and the probe beam. The pump beam after being modulated by an optical chopper is focused on the THz emitter (a second-order nonlinear optical medium), which releases a subpicosecond pulse of THz radiation in response to the incident femtosecond near infrared laser pulse. The generated THz radiation is focused onto a detector using two off-axis parabolic mirrors. The detector is an electrooptic crystal. The probe beam gates the detector, whose response is proportional to the amplitude and sign of the electric field of the THz pulse. By changing the time delay between the pump and the probe beams by means of an optical delay stage, the entire time profile of the THz transient can be traced.

Electrooptic detection of THz transients is possible when the THz radiation pulse and the probe beams coincide in a copropagating geometry inside the electro-optic crystal. A pellicle beam splitter is put in the THz beam line for this purpose. As the THz pulse and probe beam copropagate through the electrooptic crystal, a phase modulation is induced on the probe beam which depends on the electric field of the THz radiation. The phase modulation of the probe beam is analyzed by a quarter wave ($\lambda/4$) plate and the beam is then split into two beams of orthogonal

polarizations by a Wollaston prism. At this point, the phase modulation of the probe beam is converted to an intensity modulation of the two orthogonal polarizations of the probe beam, which are then steered into a pair of photodiodes. A lock-in amplifier subsequently detects the difference in probe laser light intensities measured by the photodiodes.

Next, the key aspects of the nonlinear optical processes involved in the generation and detection of short pulses of THz-frequency radiation are discussed in depth.

2.2 OPTICAL RECTIFICATION AND LINEAR ELECTROOPTIC EFFECT

Optical rectification and the linear electrooptic effect (Pockels' effect) are nonlinear optical techniques for the generation and detection of freely propagating subpicosecond THz-frequency radiation pulses.

Generally, optical rectification refers to the development of a DC or low-frequency polarization when intense laser beams propagate through a crystal. The linear electrooptic effect describes a change of polarization of a crystal from an applied electric field. Optical rectification and the linear electrooptic effect occur only in crystals that are not centrosymmetric. However, optical rectification of laser light by centrosymmetric crystals is possible if the symmetry is broken by a strong electric field. Furthermore, generation and detection of THz-radiation pulses by optical rectification and the Pockels' effect require that the crystals are sufficiently transparent at THz and optical frequencies.

Freely propagating subpicosecond THz-radiation pulses are generated by optical rectification of femtosecond (fs) near infrared laser pulses in crystals with appropriate nonlinear optical properties for this process. The detection of freely propagating THz-radiation pulses is performed by measuring the phase modulation of an fs near infrared laser pulse propagating through an electrooptic crystal simultaneously with a THz-radiation pulse. The electric field of the THz radiation induces a phase modulation of the fs laser pulse through the linear electrooptic effect.

In the following section, the theory of optical rectification and the linear electrooptic effect is discussed. The discussion of theory is limited to material we consider useful for the reader to get a general idea of the underlying physics of THz pulse generation and detection by nonlinear optical techniques and to equations that are relevant to the implementation of the techniques in the laboratory. Our discussion mainly follows the original work by pioneers in the field.

First, DC optical rectification of 694 nm continuous-wave laser radiation in potassium dihydrogen phosphate and potassium dideuterium phosphate was demonstrated experimentally by Bass et al. in 1962.[22] After that, monochromatic THz-radiation generation at 3 THz by low-difference frequency mixing of near-infrared (nir) laser radiation ($\lambda_{nir} = 1.059–1.073$ Nm) in quartz was achieved in 1965 by Zernike and Berman.[23] Yang et al. demonstrated generation of broadband (0.06–0.36 THz) freely propagating THz-radiation pulses by optical rectification of picosecond Nd: glass laser pulses in $LiNbO_3$ in 1971.[8] Eventually, Hu et al. produced free-space THz-frequency radiation with a bandwidth of 1 THz by optical rectification of femtosecond CPM dye laser pulses in $LiNbO_3$ in 1990.[10]

In 1893, Friedrich Pockels discovered the linear electrooptic effect.[24] Subsequently, the phase modulation of optical laser light at microwave frequencies using the linear electrooptic effect was demonstrated in 1962 by Harris et al.[25] Then, Valdmanis and coworkers built the first electrooptic sampling system with picosecond resolution for the measurements of ultrafast electrical transients in 1982.[26] Finally, electrooptic sampling of freely propagating THz-radiation pulses was demonstrated in 1995 by Wu and Zhang[27] and in 1996 by Jepsen et al.[28] and Nahata et al.[29]

An excellent description of laser light modulation based on the linear electrooptic effect is given by Yariv.[30] Rigorous quantum mechanical calculations of optical rectification were carried out by Armstrong et al.[31] Previous reviews of nonlinear generation and detection of sub-picosecond THz-radiation pulses were published by Bonvalent and Joffre,[32] Shen et al.,[33] and Jiang and Zhang.[34]

The discussions of optical rectification and the Pockels' effect begin by considering scalar relationships of polarization P, electric susceptibility, and electric field E.[35]

$$P = \chi(E)\, E \tag{2.1}$$

The electric polarization P of a material is proportional to the applied electric field E. Here, $\chi(E)$ is the electric susceptibility. The nonlinear optical properties of the material are described by expanding $\chi(E)$ in powers of the field E.

$$P = (\chi_1 + \chi_2 E + \chi_3 E^2 + \chi_4 E^3 + \ldots)E \tag{2.2}$$

Optical rectification and the linear electrooptic effect are second order nonlinear optical effects P_2^{nl} and described by the $P_2^{nl} = \chi_2 E^2$ term in the expansion.

For example, consider an optical electric field E described by $E = E_0 \cos \omega t$. In this case, the second-order nonlinear polarization P_2^{nl} consists of a dc polarization $\chi_2 E_0^2/2$ and a polarization with a $\cos 2\omega t$ dependence.

$$P_2^{nl} = \chi_2 E^2 = \chi_2 \frac{E_0^2}{2}(1 + \cos 2\omega t) \tag{2.3}$$

The DC polarization results from the rectification of the incident optical electric field by the second-order nonlinear electric susceptibility of the material. The polarization with the $\cos 2\omega t$ dependence describes second harmonic generation. This nonlinear optical process is not relevant to the generation and detection of THz radiation by nonlinear optical techniques and therefore not discussed further.

Similarly, consider two optical fields oscillating at frequencies $E_1 = E_0 \cos \omega_1 t$ and $E_2 = E_0 \cos \omega_2 t$.

$$P_2^{nl} = \chi_2 E_1 E_2 = \chi_2 \frac{E_0^2}{2}[\cos(\omega_1 - \omega_2)t + \cos(\omega_1 + \omega_2)t] \tag{2.4}$$

In this case, the DC second-order nonlinear polarization P_2^{nl} consists of a term $P_2^{\omega 1-\omega 2}$ proportional to the difference frequency $\omega_1 + \omega_2$ and a term $P_2^{\omega 1+\omega 2}$ proportional to the sum frequency $\omega_1 + \omega_2$. The production of THz radiation by optical rectification relies on low difference frequency generation and is described by the

term $P_2^{\omega 1-\omega 2}$. Again, sum frequency generation $P_2^{\omega 1+\omega 2}$ is not relevant to generation of THz radiation by nonlinear optical techniques.

In the same way, generation of THz-radiation pulses from optical rectification of fs laser pulses is based on difference frequency mixing of all frequencies within the bandwidth $\Delta\omega$ of an fs near infrared laser pulse.

Specifically, an fs pulse Δt is characterized by a large frequency bandwidth $\Delta\omega$. The bandwidth of the laser pulse is described by a Gauss function of width $1/4\Gamma$.[36]

$$E(\omega) \propto \exp\left(-\frac{(\omega-\omega_0)^2}{4\Gamma}\right) \tag{2.5}$$

In the time domain, the fs laser pulse is described by an optical field oscillating at frequency ω_0 with a time dependence described by a Gauss function.

$$E(t) = E_0 \exp(i\omega_0 t)\exp(-\Gamma t^2) \tag{2.6}$$

The bandwidth of the THz-radiation pulse is determined by difference frequency generation by all frequencies within the bandwidth of the fs laser pulse. The time profile of the radiated THz pulse from optical rectification of the fs laser pulse is proportional to the second time derivative of the difference frequency term $P_2^{\omega 1-\omega 2}$. The time dependence of $P_2^{\omega 1-\omega 2}$ is determined by the Gaussian time profile of the optical laser pulse.

The physics of the linear electrooptic effect is described by the same term $P_2^{n1} = \chi_2 E^2$ in the expansion of $\chi(E)$ as optical rectification. To understand the relationship between optical rectification and the Pockels' effect, it is now necessary to describe polarization P and electric field E by vectors and the susceptibility χ by a third rank tensor.

Quantum mechanical calculations of the polarization for the case of two laser beams with frequencies ω_2, ω_1 present in a crystal demonstrate that the ith component of the second-order nonlinear polarization $p_i^{\omega 1-\omega 2}$ is related to the components j and k of the electrical fields $E_j^{\omega 1}$ and $E_k^{\omega 2}$ via the susceptibility tensor component $\chi_{ijk}^{\omega 1-\omega 2}$ [35]

$$p_i^{\omega_1-\omega_2} = \chi_{ijk}^{\omega_1-\omega_2} E_j^{\omega_1} E_k^{\omega_2} \tag{2.7}$$

DC optical rectification and the linear electrooptic effect result from Equation 2.7 considering the limits of $\omega_2 -> \omega_1$ and $\omega_2 -> 0$, respectively.

$$\omega_2 \to \omega_1 \qquad p_i^0 = \chi_{ijk}^0 E_j^{\omega_1} E_k^{\omega_1} \tag{2.8}$$

$$\omega_2 \to 0 \qquad p_i^{\omega_1} = \chi_{ijk}^{\omega_1} E_j^{\omega_1} E_k^0 \tag{2.9}$$

Equations 2.8 and 2.9 demonstrate that a strong electric field at frequency ω_1 gives rise to a dc polarization p_i^0 and a DC electric field E_k^0 changes the polarization $p_i^{\omega 1}$ at frequency ω_1.

Further calculations demonstrate that $\chi^{0}{}_{ijk}$ is equal to $\chi^{\omega 1}{}_{jik}$. Therefore, the third rank tensors are identical under simple interchange of indices as well as frequencies. This demonstrates the identity of optical rectification and the linear electrooptic effect. As a result of this identity, it is possible to estimate the magnitude of optical rectification from the linear electrooptic coefficients of a material.

The most widely employed crystals for nonlinear optical generation and detection of THz radiation are ZnTe, gallium phosphide (GaP), and GaSe. ZnTe and GaP exhibit zincblende structure and $\bar{4}3m$ point group symmetry. GaSe is a hexagonal crystal with $\bar{6}2m$ point group symmetry. All three crystals are uniaxial. Uniaxial crystals have only one axis of rotational symmetry referred to as the c-axis or optical axis of the crystal. The efficacy of ZnTe, GaP, and GaSe for nonlinear optical THz generation and detection is rated by the linear electrooptic coefficient of the materials. The linear electroptic coefficients for ZnTe, GaP, and GaSe are listed in Table 2.1. The relationship between susceptibility tensor elements describing optical rectification $\chi_{ijk}{}^{0}$ and linear electrooptic effect $\chi_{jik}{}^{\omega}$ is:

$$\chi_{ijk}{}^{0} + \chi_{ikj}{}^{0} = \frac{1}{2}\chi_{jik}{}^{\omega} \tag{2.10}$$

and the relationship between the linear electrooptic coefficient r_{jki} and the linear electrooptic effect tensor element $\chi_{jik}{}^{\omega}$ is:

$$r_{jki} = -\left(\frac{4\pi}{n_0{}^2 n_e{}^2}\right)\chi_{jik}{}^{\omega} \tag{2.11}$$

Efficient generation and detection of THz radiation by optical rectification and the Pockels' effect require single crystals with high second-order nonlinearity or large electrooptic coefficients, proper crystal thickness and proper crystal orientation with respect to the linear polarization of the THz radiation. The surfaces of the crystals should be optically flat at the laser excitation wavelengths and of high crystalline quality (e.g., low levels of impurities, structural defects, and intrinsic stress).

The bandwidth of an electrooptic crystal for THz generation and detection is determined by the coherence lengths and optical phonon resonances in the material.

TABLE 2.1
Electrooptic Coefficients of Some Commonly Used Terahertz Emitters and Detectors

Material	Structure	Point Group Symmetry	Electrooptic Coefficient (pm/V)
ZnTe	Zincblende[30]	$\bar{4}3m$[30]	$r_{41} = 3.9$[30]
GaP	Zincblende[30]	$\bar{4}3m$[30]	$r_{41} = 0.97$[30]
GaSe	Hexagonal [53]	$\bar{6}2m$[30]	$r_{41} = 14.4$[76]

Infrared active optical phonon resonances result in strong absorption of electromagnetic radiation at the absorption frequencies. The phonon absorption bands (optical phonons) of a material in the THz frequency range are not available for THz generation and detection.

If the refractive indices of the near infrared laser excitation frequency and the THz radiation are identical, then the bandwidths of the THz radiation depend only on the pulse width of the incident femtosecond near infrared laser beam. Furthermore, the strength of emission and sensitivity of THz detection would increase similarly for all frequencies within the bandwidth with increasing crystal thickness.

However, the refractive indices for the near infrared laser frequency and THz frequency are generally not identical. Consequently, electromagnetic waves at THz and near infrared frequencies travel at slightly different speeds through the crystal. The efficacy of nonlinear optical THz generation and detection decreases if the mismatch between the velocities becomes too large. The distance over which the slight velocity mismatch can be tolerated is called the coherence length. As a result, efficient THz generation and detection at a given frequency only occur for crystals that are equal in thickness or thinner than the coherence length for this frequency.

The coherence length in case of pulsed near-infrared laser radiation is defined as:[11]

$$l_c\left(\omega_{THz}\right) = \frac{\pi c}{\omega_{THz} \mid n_{opt\ eff}(\omega_0) - n_{THz}(\omega_{THz}) \mid} \tag{2.12}$$

with

$$n_{opt\ eff} = n_{opt}(\omega) - \lambda_{opt}\left(\frac{\partial n_{opt}}{\partial \lambda}\right)\Bigg|_{\lambda_{opt}} \tag{2.13}$$

In Equations 2.12 and 2.13, c is the velocity of light, $\omega_{THz} = 2\pi/\upsilon_{THz}$ the THz frequency, ω_0 is the near infrared excitation frequency n_{THz} the refractive index at THz frequencies, n_{opt} the index of refraction at near infrared wavelength λ_{opt}, and $n_{opt\ eff}$ the group velocity refractive indices of the femtosecond near infrared laser pulse.

THz emission strength of a crystal and sensitivity of an electrooptic THz detector are proportional to the thickness of the crystal. However, the bandwidth of the THz emitter crystal and bandwidth of the THz detector crystal also depend on the crystal thickness. Generally THz emission strength and THz emission bandwidth for a crystal have a reciprocal relationship. The THz emission bandwidth increases when the crystal becomes thinner. The THz emission strength decreases when the crystal becomes thinner. The same rule applies to the sensitivity of an electrooptic THz detector and the detector bandwidth. Thinner crystals have a higher bandwidth but lower sensitivity than thicker crystals and vice versa.

For efficient generation of THz radiation by optical rectification of femtosecond laser pulses from zincblende structure crystals, it is important to select the proper orientation of the crystal with respect to the linear polarization of the laser beam. The preferred crystal orientations of selected materials are discussed in Sections 2.3 and 2.4.

In case of the longitudinal linear electrooptic effect, the electric field is applied parallel to the direction of propagation of the optical probe laser beam. In case of the transverse linear electrooptic effect, the electric field is applied perpendicular to the direction of propagation of the optical probe beam. Detection of THz radiation pulses is generally performed using the geometry of the transverse electrooptic effect.

The amplitude and phase of the subpicosecond THz-radiation pulse are measured by recording the phase change of femtosecond near infrared laser pulses traveling collinearly and simultaneously with the THz radiation pulses through the electrooptic crystal. The electric field of the THz radiation induces a change of the index of refraction of the crystal via the linear electrooptic effect such that the material becomes birefringent. The phase retardation Γ between the ordinary and extraordinary ray after propagating through the birefringent crystal is proportional to the amplitude and phase of the THz electric field E, the crystal thickness l, the linear electrooptic coefficient r_{14}, the index of refraction of the crystal at the near infrared laser frequency n_o, and the near-infrared wavelength λ.[30]

$$\Gamma \propto \frac{1}{\lambda} l n_0^3 r_{41} E_{THz} \tag{2.14}$$

Furthermore, the phase retardation also depends on the orientation of the crystal and directions of polarization of the THz radiation pulse and the near infrared laser pulse.[37] For $\bar{4}3m$ zincblende structure crystals, preferred directions of the THz electric field E_{THz}, optical field E_{opt}, and crystal orientation are discussed in Sections 2.3 and 2.4.

The temporal profile of the THz radiation is mapped out in time by delaying the much shorter femtosecond near infrared laser pulse with respect to the THz radiation pulse and measuring the phase retardation as a function of the delay between THz radiation pulse and optical probe pulse.

2.3 EXPERIMENTAL RESULTS OF TERAHERTz-FREQUENCY RADIATION GENERATION BY OPTICAL RECTIFICATION OF FEMTOSECOND LASER PULSES

In this chapter, we review the experimental results for generation of THz radiation pulses based on optical rectification. Several nonlinear optical materials have been reported to generate THz radiation by optical rectification of a femtosecond near infrared laser pulse. Table 2.2 lists the various crystals investigated for generation of THz radiation by optical rectification. For the sake of organization, the experimental results will be divided into three broad material categories: semiconductors, inorganic electrooptic crystals and organic electrooptic crystals, and the characteristics of the emitted THz radiation will be discussed in brief under each material category. The performance of various emitters will be discussed on the basis of bandwidth and amplitude of the emitted THz radiation. We conclude our discussion by presenting recent experimental developments in THz emitter research.

TABLE 2.2
Materials Used for Generation of Terahertz Optical Rectification

Semiconductors	Inorganic Electrooptic Crystals	Organic Electrooptic Crystals
GaAs	$LiNbO_3$	4-N-methylstilbazolium tosylate (DAST)
InP	$LiTaO_3$	N-benzyl-2-methyl-4-nitroaniline (BNA)
CdTe		(-) 2-(α-methylbenzyl-amino)-
InAs		5-nitropyridine (MBANP)
InSb		electrooptic polymers
GaP		
ZnTe		
ZnCdTe		
GaSe		

2.3.1 Materials

2.3.1.1 Semiconductors

A significant amount of research dating back as early as the 1970s has explored the generation of THz radiation by optical rectification of pico- and femtosecond optical pulses in nonlinear optical crystals. Experimental work in the early 1990s reported that THz-frequency radiation could also be generated by femtosecond optical pulses incident on a semiconductor surface.[38,39] This observation was initially explained as the dipole radiation of a time-varying current resulting from photo-excited charge carriers in the depletion field near the semiconductor surface.[39–41] Although the ultrafast photocarrier transport model successfully explained the transverse magnetic polarization of the emitted THz radiation and the observed emission maxima for Brewster angle incidence, the intensity modulation of the emitted THz radiation observed when the crystal was rotated about its surface normal indicated that there was more than one mechanism responsible for the generation of THz radiation. In 1992, Chuang et al.[42,43] proposed a theoretical model based on optical rectification of femtosecond laser pulses at semiconductor surfaces, which successfully explained all of the earlier experimental observations. The investigation of the physics of optical rectification indicates that depending on the optical fluence, the THz radiation generation by optical rectification is either a second-order nonlinear optical process governed by the bulk second-order susceptibility tensor χ_2, or a third-order nonlinear optical process whereby a second-order nonlinear susceptibility results from the mixing of a static surface depletion field and the third-order nonlinear susceptibility tensor χ_3.[41,44]

THz radiation generation from optical rectification of femtosecond laser pulses has been reported from <100>, <110>, and <111>-oriented crystals with zincblende structure commonly displayed by most III–V (and some II–VI) semiconductors. These crystals have a cubic structure with $\bar{4}3m$ point group symmetry and only one independent nonlinear optical coefficient, namely $r_{41} = r_{52} = r_{63}$.[30] Theory predicts that for <100>-oriented zincblende crystals, there is no optical rectification field at normal incidence (as the nonvanishing second-order optical coefficients r_{41}, r_{52}, and

r_{63} are not involved), whereas a three-fold rotation symmetry about the surface normal may be observed for <110> and <111> orientations. Experimental studies conducted on <100>, <110>, and <111> oriented GaAs, CdTe, and indium phosphide (InP) crystals[13,17,41] and <110> GaP crystal[45] are in excellent agreement with the theoretical results providing evidence that second-order bulk optical rectification is the major nonlinear process under the condition of moderate optical fluence (~nJ/cm^2) and normal incidence on unbiased semiconductors. A dramatic variation in the radiated THz signal along with polarity reversal is observed in <110> and <111> CdTe and GaAs crystals, as the incident photon energy is tuned near the bandgap.[13,17,41] This phenomenon can be explained as the dispersion of the nonlinear susceptibility tensor near the electron resonance state.[13,41]

THz generation by optical rectification has recently also been reported from narrow bandgap semiconductors such as indium arsenide (InAs) and indium antimonide (InSb) at high optical fluence (1–2 mJ/cm^2) and off-normal incidence.[44,46–50] Experimental results of THz emission from <100> InSb crystal and <100>, <110>, and <111> InAs crystal for both n- and p-type doping were examined.[44,49] A pronounced angular dependence of the emitted THz radiation on the crystallographic orientation of the samples as well as on the optical pump beam polarization was observed. The experimental results are in good agreement with the theory, which predicts that for high excitation fluence, THz emission from narrow band gap semiconductors results primarily from surface electric field-induced optical rectification with small bulk contribution.[50] This observation is in contrast with the earlier results obtained for wide bandgap semiconductors such as GaAs, in which the THz emission is primarily dominated by strong bulk contribution. The anomaly can be explained in the light of the theoretical calculations by Ching and Huang[51] whereby narrow bandgap III–V semiconductors (InAs and InSb) are predicted to have third-order nonlinear susceptibilities (χ_3) several orders of magnitude higher than those of larger bandgap semiconductors.

Among the zincblende crystals, perhaps the most popular candidate for generation of THz radiation by optical rectification is ZnTe. Nahata et al.[11] first reported THz generation in ZnTe in an experiment that used a pair of ZnTe crystals for both generation and detection of THz radiation. In their work, a <110> ZnTe crystal was pumped by 130 femtosecond pulses at 800 nm from a mode-locked Ti:sapphire laser. The Fourier spectrum of the temporal waveform demonstrated a broad bandwidth with useful spectral information beyond 3 THz. Subsequently, Han et al.[12] reported a higher frequency response of 17 THz limited only by a strong phonon absorption at 5.3 THz. Systematic studies have also been conducted on THz emitter application of cadmium zinc telluride ternary crystals with varying Cd composition. It has been reported[18,52] that the optimum Cd composition x = 0.05 enhances THz radiation as well as crystal quality of ZnTe.

Apart from the zincblende crystals described earlier, GaSe is a promising semiconductor crystal that has been exploited recently for THz generation with an extremely large bandwidth of up to 41 THz.[15,53] GaSe is a negative uniaxial layered semiconductor with a hexagonal structure characteristic of $\bar{6}2m$ point group and a direct bandgap of 2.2 eV at 300 K. The crystal has a large nonlinear optical coefficient (54 pm/V),[53] high damage threshold, suitable transparent range, and low absorption coefficient, which make it an attractive option for generation of

broadband mid infrared electromagnetic waves. For broadband THz generation and detection using a sub-20 fs laser source, GaSe emitter-detector system performance is comparable to or better than the use of thin ZnTe crystals. Using GaSe crystals of appropriate thickness as emitter and detector it is also possible to obtain a frequency-selective THz wave generation and detection system. The disadvantage of GaSe lies in the softness of the material that makes it fragile during operation.

2.3.1.2 Inorganic Electrooptic Crystals

In 1971 Yang et al. first demonstrated the generation of THz radiation by optical rectification of picosecond optical pulses in inorganic electrooptic materials. In their experiment they observed THz radiation from a $LiNbO_3$ crystal illuminated by picosecond optical pulses from a mode-locked Nd:glass laser.[8] In the late 1980s, Auston and coworkers reported THz radiation generation by optical rectification in $LiTaO_3$ with spectral bandwidth as high as 5 THz.[54] A major drawback in this experiment was the difficulty in extracting the THz pulses from the generating crystal because of total internal reflection owing to small critical angle (and high static dielectric constant) in $LiTaO_3$. In their later publications Auston et al. reported an approach that minimized the reflection loss and permitted the extraction of the THz radiation into free space.[10] Zhang et al.[9] later measured and calculated optical rectification from $LiNbO_3$ and y-cut $LiTaO_3$ under normal incident optical excitation. The spatio-temporal shape of the radiated THz pulse was found to be similar for both materials with $LiNbO_3$ emitting a stronger signal because of a smaller dielectric constant and hence smaller reflection losses at the crystal boundary. The maximum signal obtained from $LiTaO_3$ was found to be 185 times smaller than that emitted by a 4-N-methylstilbazolium tosylate (DAST) organic crystal.[19]

2.3.1.3 Organic Electrooptic Crystals

Organic crystals have been a recent source of interest as THz emitters as they have been reported to generate stronger THz signals than commonly used semiconductors or inorganic electrooptic emitters owing to their large second-order nonlinear electric susceptibility. Zhang et al.[19] first reported THz optical rectification from an organic crystal, dimethyl amino DAST, which is a member of the stilbazolium salt family. Electrooptic measurements at 820 nm have reported a high electrooptic coefficient (>400 pm/V).[19]

In their work on THz emission by optical rectification of femtosecond laser pulses in DAST, Zhang et al. observed a strong dependence of the radiated THz field amplitude on sample rotation about the surface normal, for both parallel and perpendicular orientations of the incident optical pump beam. The angular dependence was in excellent agreement with the predicted theory, with the maximum signal occurring for the angle at which the optical polarization, the crystal polar "*a*" axis and the detector dipole axis, were aligned in the same direction.[19] Zhang and coworkers[19] also reported that with a 180-mW optical pump beam focused to a 200-μm diameter spot, the best DAST sample provided a detected THz electric field that was 185 times larger than that obtained from an $LiTaO_3$ crystal and 42 times larger than GaAs and InP crystals under the same experimental conditions. DAST has also been shown to

perform well at higher frequencies with an observable bandwidth up to 20 THz from a 100-μm DAST crystal showing a six-fold increase over that reported from a 30-μm ZnTe crystal under similar experimental conditions.[55] The frequency spectrum of DAST shows a characteristic strong absorption line at 1.1 THz (from TO phonon resonance) along with some additional absorption lines between 3 and 5 THz. The latter (with the exception of the line at 5 THz) are significantly weaker than the absorption line at 1.1 THz, such that the THz amplitude at these frequencies is still well above the noise level.[56]

Nahata et al.[57] advocated the use of organic compounds in polymeric forms for THz-frequency radiation generation instead of single crystals as these compounds offer significant advantages over single crystals. In particular they are easily processable, can be poled to introduce noncentrosymmetry and have higher nonlinear coefficients than inorganic materials. In their experiment Nahata and coworkers used a copolymer of 4-*N*-ethyl-*N*- (2-methacryloxyethyl) amine-4′-nitro-azobenzene (MA1) and methyl methacrylate (MMA) (commonly known as MA1:MMA) for generation of THz radiation via optical rectification. The radiated field amplitude from a 16-μm thick sample (electrooptic coefficient ~11 pm/V) was found to be four times smaller than that observed from a 1-mm thick y-cut $LiNbO_3$ crystal. However, the coherence length of the polymer was reported to be 20 times larger. Nahata and coworkers suggested that the conversion efficacy relative to $LiNbO_3$ could be substantially improved using available polymers with six times the nonlinear coefficient and millimeter-thick films poled at high fields. This could be easily created by a dielectric stack of thin-poled films.[58]

After the success of DAST and MA1:MMA as THz emitters, Hashimoto et al. reported THz emission via optical rectification from organic single crystals of N-substituted (N-benzyl, N-diphenylmethyl, and N-2 naphthylmethyl) derivatives of 2-methyl-4-nitroaniline.[59] While no substantial emission was observed from N-diphenylmethyl and N-2 naphthylmethyl derivatives (owing to the strong phonon modes existing in the range 0 to 2.5 THz), the integrated intensity of the THz radiation emitted by N-benzyl-2-methyl-4-nitroaniline (BNA) was as intense as that by the DAST crystal under similar experimental conditions. The dynamic range for BNA is limited to 2.1 THz because of a strong phonon mode that exists around 2.3 THz. Kuroyanagi and coworkers[60] later reported improved signal intensity (about three times greater than that generated by ZnTe) and increased bandwidth (up to 4 THz) from highly purified BNA crystals.

Although DAST and BNA have been reported to perform better than ZnTe when used for THz generation by optical rectification, the THz electric fields generated by these crystals are more complicated in both time and frequency domains. Phonon bands in these crystals also result in the production of smaller range of frequencies than ZnTe. Recent investigations of a range of organic molecular crystals revealed that the crystal (–) 2-(α-methylbenzyl-amino)-5-nitropyridine (MBANP) is superior to ZnTe when used for optical rectification at 800 nm.[61] MBANP crystallizes in $P2_1$ monoclinic[62] and has the advantage of being relatively easy to grow in single crystals, probably because of its L-shaped structure and strong H bonding in certain directions as well as a suitable habit.[61] Optical rectification of 800-nm pulses in <001>-oriented MBANP resulted in THz pulses that are very similar to those

produced by ZnTe both in frequency and time domain. However, MBANP produces a signal that is an order of magnitude higher because of its larger electrooptic coefficient (18.2 pm/V at 632.8 nm).[63] Several other crystals similar to MBANP have also been studied.[61] It was found that 4-(N, N-dimethylamino)-3-acetamidonitrobenzene and 4-nitro-4′-methylbenzylidene aniline (NMBA) produced THz pulses through optical rectification of 800-nm pulses of comparable strength to MBANP. While NMBA is easy to grow, 4-(N, N-dimethylamino)-3-acetamidonitrobenzene is much more difficult owing to its needle-like habit, and obtainable crystal size is limited. Strong phonon band absorption also limits the power in the range 1.6 to 3 THz, which makes these crystals unsuitable for high-frequency applications.

We have thus reviewed THz optical rectification from a variety of materials including semiconductors and inorganic and organic electrooptic crystals. The performance of these emitters in terms of bandwidth has been summarized in Table 2.3. ZnTe is the most popular choice for THz generation by optical rectification because it can generate extremely short and high-quality THz pulses. Organic crystals have been of recent interest owing to their higher electrooptic coefficient and enhanced capacity to generate stronger signals than the commonly used ZnTe. However, the THz fields generated by organic crystals such as DAST and more recently BNA are more complicated in both time and frequency domain. Low-frequency phonon bands also limit the bandwidth in these crystals than compared with ZnTe. Organic crystals also have a large naturally occurring birefringence, which complicates their application.[55] This has resulted in ZnTe remaining the THz generator of choice. The comparative performance of a ZnTe THz emitter pumped by an amplified titanium sapphire laser system is shown in Figure 2.2.[64]

The choice of a suitable THz emitter also largely depends on the operating conditions. As mentioned previously, to achieve reasonable efficacy for nonlinear optical processes, long interaction length and appropriate phase matching conditions must be met. The phase matching condition is satisfied when the phase of the THz wave travels at the group velocity of the optical pulse. In the case of ZnTe, the phase matching condition and the subsequent enhancement of coherence length are achieved at 800 nm, making it the most suitable electrooptic crystal for THz wave emission and detection using a Ti:sapphire laser system with a center wavelength of 800 nm.

TABLE 2.3
Bandwidth Performances of Some Common Terahertz Emitters

Material	Experimental Bandwidth (THz)	Lowest Optical Phonon Resonance (THz) at 300 K	Incident Pulse Wavelength (nm)	Incident Pulse Width (fs)	Detection Scheme
GaAs	40[12]	8.02[71]	800[12]	12[12]	Electrooptic
GaSe	41[15]	7.1[15]	780[15]	10[15]	Electrooptic
ZnTe	17[12]	5.4[12]	800[12]	12[12]	Electrooptic
GaP	3.5[45]	10.96[71]	1055[45]	300[45]	PC antenna
DAST	20[55]	1.1[56]	800[55]	15[55]	Electrooptic
BNA	2.1[59]	2.3[59]	800[59]	100[59]	Electrooptic

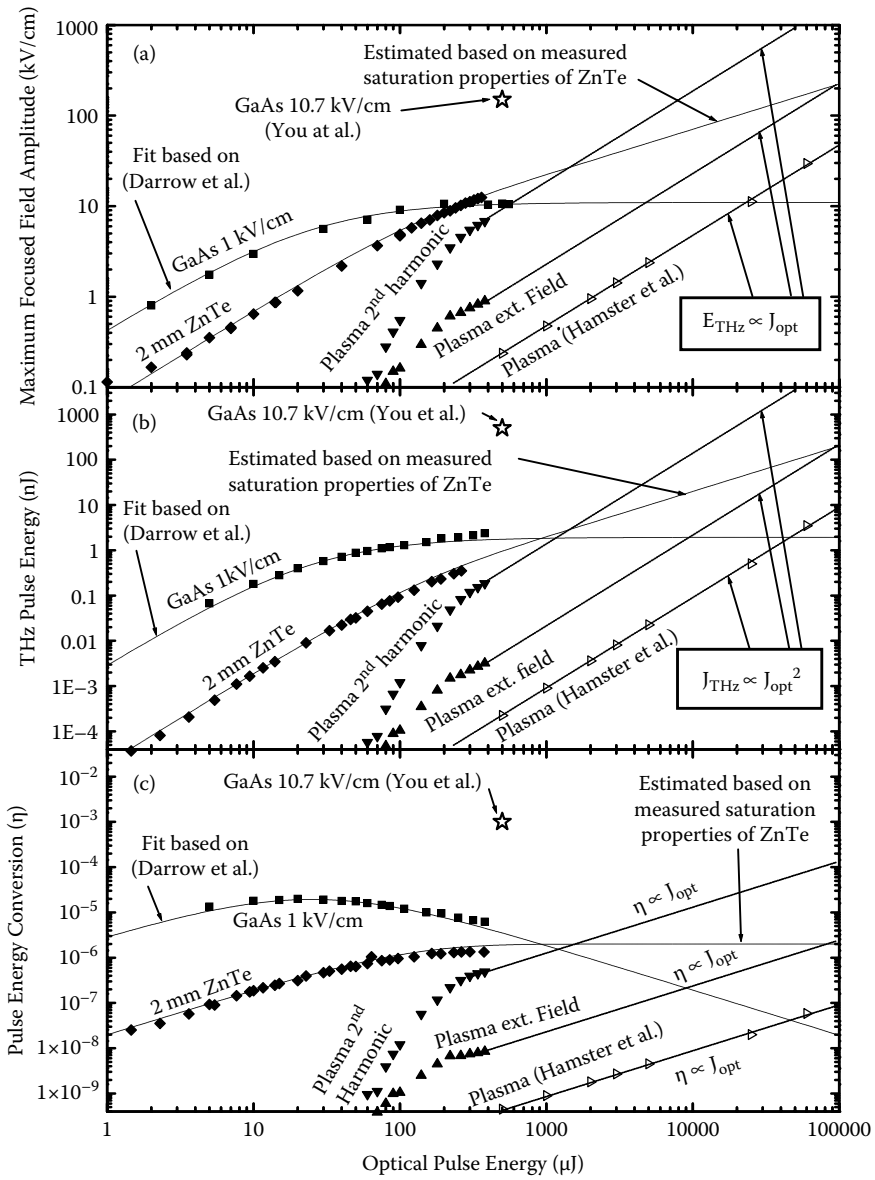

FIGURE 2.2 Comparison of the THz emission efficacy of a 2-mm ZnTe crystal with other types of THz emitters: (a) the focused peak electric field, (b) the THz pulse energy, and (c) the energy conversion efficacy are displayed as a function of the energy per pulse of the femtosecond near infrared pump laser. (From Loeffler T., *Semicond. Sci. Technol.* 20, S140, 2005, IOP Publishing. With permission.)

However, the large size of these lasers prevents them from being used in portable THz systems. To build a compact, integrated, and sensitive THz spectroscopy or THz imaging system, it has thus become crucial to develop a THz wave generation and detection technique coupled to an optical fiber cable. The erbium (Er)- and ytterbium (Yb)-doped fiber lasers operating at 1,550 nm and 1,000 nm, respectively, are especially attractive from this viewpoint. The large velocity mismatch and consequently a small coherent length, however, make ZnTe unsuitable for application at these wavelengths. Although GaP and CdTe have been suggested as potentially compatibles emitters for Yb-doped laser systems operating at 1,000 nm, GaAs is an excellent candidate for THz wave emission with erbium-doped fiber lasers. Calculations[17] show that the phase matching condition is satisfied at 1,050 nm and 1 THz in CdTe crystals resulting in an enhancement of coherence length, whereas GaAs crystal phase matching occurs at 1,330 nm. This optical wavelength in GaAs is the longest among all binary semiconductors.[14] Even at 1,550 nm, the coherence length still retains a large value, thus enabling GaAs to be used a suitable emitter in this wavelength range. GaAs also has the added advantage of having its lowest phonon resonance lying at higher THz frequencies (10 THz) and consequently increased bandwidth capability. The coherence length of some organic crystals such as BNA is also quite large in the long wavelength regime; however, because of the difficulties highlighted previously, organic crystals have not gained popularity as THz emitters.

2.3.2 Recent Developments

The increasing interest in the development of novel THz sources has stimulated in-depth studies of microscopic mechanisms of THz field generation in conventional semiconductors,[38–53] electrooptic materials,[55–63] and an extensive search for new materials to be employed in THz generation and detection. We conclude our discussion on THz emitters by highlighting some recent developments in THz emitter research.

The THz emission from nonresonant optical rectification discussed in earlier sections resulted from dipolar excitations from such materials as GaAs, ZnTe, and $LiNbO_3$. THz emission may also result from nondipolar excitations. Emission via optical rectification of femtosecond laser pulses in $YBa_2Cu_3O_7$,[65] single crystals of iron (Fe),[66] and films consisting of nanosized graphite crystallites[67] was observed and was found to have resulted from quadrupole magnetic dipole nonlinearities.

For Fe, which crystallizes in a body-centered cubic lattice, optical rectification is forbidden by lattice symmetry. A nonvanishing second-order optical nonlinearity can, however, result from an electric quadrupole magnetic dipole contribution, surface nonlinearity or sample magnetization. Each of these contributions to the second-order nonlinear electric susceptibility has a characteristic dependence on sample azimuth and optical pump pulse polarization for a given crystal orientation. The THz emission reported from Fe was found to be approximately three orders of magnitude weaker than that from a 1-mm thick <110> ZnTe crystal under the same optical excitation conditions.

THz emission from metals such as gold and silver has also come to light recently.[20,21] Although second harmonic generation had been reported from metal surfaces as early as the 1960s, optical rectification of laser light had not been reported until recently. Kadlec et al.[20,21] generated intense THz emission by optical

rectification of p-polarized 810-nm laser pulses at a fluence of 6 mJ/cm^2 in gold films. The THz amplitude was found to scale quadratically with optical fluence for values up to 2 mJ/cm^2. The s-polarized optical pump beam resulted in THz radiation emission, which was approximately three times weaker than the signal obtained from a p-polarized optical pump beam. THz emission from silver showed a different behavior. At the highest optical pump fluence, the emitted THz radiation was 15 times weaker than for gold and showed a linear dependence on incident pump fluence.[20] These recent experimental findings reveal the possibility of accessing a wealth of new information about nonlinear optical properties and electronic structures of metal surfaces via femtosecond optically excited THz emission measurements.

2.4 EXPERIMENTAL RESULTS OF TERAHERTZ ELECTROOPTIC DETECTION

Much research activity has been devoted to increasing the sensitivity and bandwidth of electrooptic detection of THz-frequency radiation pulses. Other than the duration of the optical probe pulse, the bandwidth of free-space electrooptic sampling is only limited by the dielectric properties of the electrooptic crystal. Electrooptic sampling of THz-frequency radiation is a powerful tool for detection of electromagnetic radiation pulses in and beyond the mid-infrared range. A variety of electrooptic materials, including semiconductors and inorganic and organic electrooptic crystals, have been tested for detector applications in THz spectroscopy. In this section, we present a brief overview of the experimental results of broadband THz electrooptic detection with various materials.

2.4.1 Materials

2.4.1.1 Semiconductors and Inorganic Crystals

In 1995, Wu and Zhang[27] first demonstrated free-space electrooptic sampling of short THz radiation pulses. In their experiment, a GaAs photoconductive emitter triggered by 150-fs optical pulses at 820 nm radiated electromagnetic waves of THz frequency. A 500-μm thick $LiTaO_3$ crystal, with its *c* axis parallel to the electric field polarization, was used as the electrooptic sampling element. To improve detection efficacy, the THz radiation beam was focused onto the detector crystal by a high-resistivity silicon lens. The temporal resolution of the detected THz transient was limited by the velocity mismatch between optical and THz frequencies. Later work by Wu and Zhang[68,69] addressed this shortcoming by careful geometric design of the radiation emitter and a special cut detector crystal. A signal-to-noise ratio of about 170:1 was obtained with a 0.3-second lock-in integration time constant.

Wu and coworkers also tested ZnTe for detector applications in a novel experimental geometry in which the optical and THz beams were made to propagate collinearly in the electrooptic crystal.[68] In this setup, a 1.5-mm thick, <110>-oriented ZnTe crystal was used as the detector with the optical probe and THz beam set parallel to the <110> edge of the ZnTe crystal for optimal electrooptic phase modulation. A signal-to-noise ratio of about 10,000:1 was obtained for a single scan using again a lock-in amplifier with time constant of 0.3 seconds. Nahata et al.[11] demonstrated a

broadband time domain THz spectroscopy system using <110>-oriented ZnTe crystals for generation of THz radiation by optical rectification and detection of THz radiation by electrooptic sampling.

An important condition for generation and detection of THz radiation by nonlinear optical techniques is the appropriate phase matching between the optical and THz pulses in the nonlinear optical crystal. For a medium with dispersion at optical frequencies, phase matching is achieved when the phase velocity of THz wave is equal to the velocity of optical pulse envelope (or the optical group velocity).[11] The data in Figure 2.8 show the effective index of refraction of ZnTe at optical wavelengths $n_{opt\ eff}$ and THz frequencies n_{THz}. The coherence length l_c of ZnTe at THz frequencies for an optical wavelength $\lambda = 780$ nm decreases as illustrated in Figure 2.3. The temporal waveform of the measured THz electric field and its Fourier amplitude and Fourier phase are displayed in Figures 2.3, 2.4, and 2.5, respectively. The peak of the THz pulse amplitude shows a three-fold rotational symmetry when the ZnTe detector crystal is rotated by 360° about an axis normal to the <110> surface. This result is inherent to all <110> and <111> zincblende crystals.[40] The broadband detection capability of ZnTe is obvious from the Fourier amplitude spectrum (Figure 2.4), which extends well beyond 2 THz. The rolloff in sensitivity for higher frequencies from phase mismatch and the shorter coherence length are in agreement with data presented in Figures 2.6, 2.7, and 2.9. A thinner crystal detects higher frequencies better than a thicker crystal. However, the detector sensitivity of a thinner crystal is reduced compared to a thicker crystal. In addition to limitations imposed by

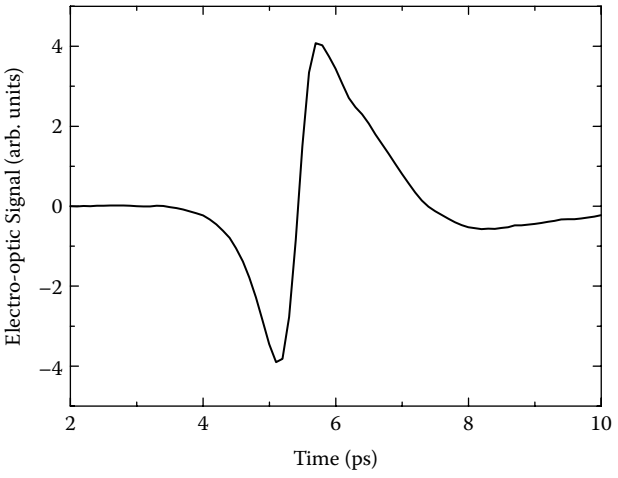

FIGURE 2.3 Time domain measurement of a THz pulse by electrooptic sampling with a ZnTe crystal 10 mm × 10mm × 1 mm in size. The THz pulse and the optical probe pulse are incident onto the surface of the ZnTe crystal parallel to the <110> plane. The optical axis of the crystal is in the <001> direction. The linear polarization of the THz radiation pulse is perpendicular to the optical axis. The linear polarization of the incident optical probe pulse is parallel to the optical axis. (Adapted from Selig, H., Elektro-optisches Sampling von Terahertz Pulsen, Hochschulschrift: Hamburg, Universitaet, Fachbereich Physik, Diplomarbeit, 7,2000. With permission.)

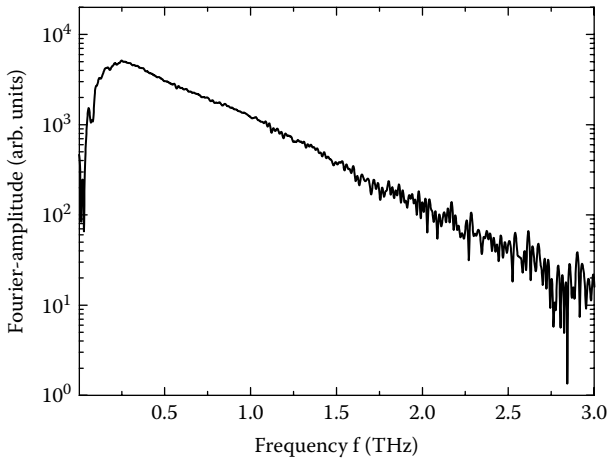

FIGURE 2.4 Fourier amplitude of the time domain measurement displayed in Figure 2.3. The bandwidth of the signal is approximately 2.75 THz. The dynamic range of the measurement is 500:1. (Adapted from Selig, Hanns, Elektro-optisches Sampling von Terahertz Pulsen, Hochschulschrift: Hamburg, Universitaet, Fachbereich Physik, Diplomarbeit, 7, 2000. With permission.)

phase mismatch, the absorption caused by a transverse optical phonon resonance at 5.4 THz[11] in ZnTe is expected to attenuate the high-frequency components of THz radiation. Later experiments by Han and Zhang[70] reported a detection bandwidth up to 40 THz using a 27-μm ZnTe detector crystal.

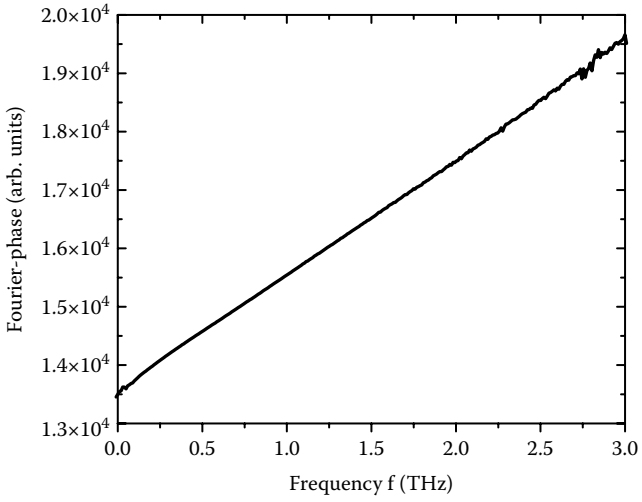

FIGURE 2.5 Fourier phase of the time domain measurement displayed in Figure 2.3. (Adapted from Selig, H., Elektro-optisches Sampling von Terahertz Pulsen, Hochschulschrift: Hamburg, Universitaet, Fachbereich Physik, Diplomarbeit, 7, 2000. With permission.)

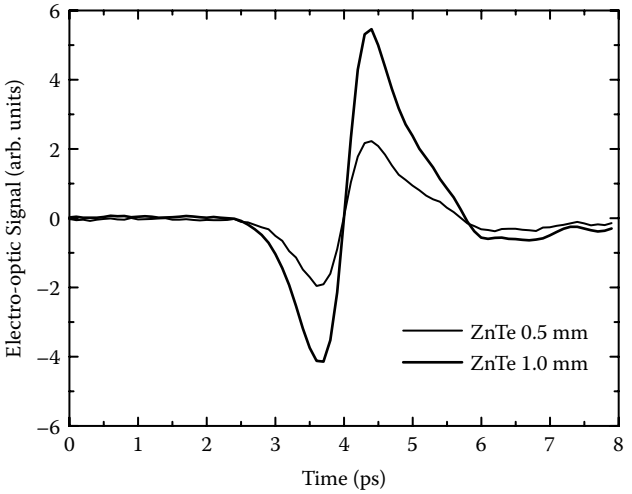

FIGURE 2.6 Time domain measurements of THz pulses by electrooptic sampling with ZnTe crystals of different thickness. For both measurements, the optical probe beam and the THz pulse both incident onto the surface of the crystals parallel to the <110> plane. The surface of the crystals is 10 mm × 10 mm. The linear polarizations of the incident THz-pulse and probe pulse are perpendicular to each other. The polarization of the probe beam is parallel to the optical axis (<001> direction). The ratio of the peak-to-peak amplitude of the THz pulses measured by the 1-mm crystal and the 0.5-mm crystal is 2.3 and scales approximately with the thickness of the two crystals (1 mm/0.5 mm = 2). The thicker ZnTe crystal exhibits a larger signal than the thinner crystal because the phase retardation $\Gamma \propto l$ is linearly proportional to the thickness l of the electrooptic crystal. (Adapted from Selig, H., Elektro-optisches Sampling von Terahertz Pulsen, Hochschulschrift: Hamburg, Universitaet, Fachbereich Physik, Diplomarbeit, 35,2000. With permission.)

Although ZnTe delivers excellent performance in the 800-nm wavelength regime, its efficacy is inherently limited by large group velocity mismatch (GVM) of 1 ps/mm[68] between optical and THz frequencies. An ideal material would be one with larger electrooptic coefficient and lower GVM. At 886 nm, GaAs has been found to possess a moderate electrooptic coefficient (25 pm/V), but a low GVM of 15 fs/mm. The electrooptic coefficient of $LiTaO_3$ was found to be comparable to that of ZnTe, but $LiTaO_3$ has a large GVM (>14 ps/mm), whereas for organic crystals such as DAST, the electrooptic coefficient is very large but GVM is comparable to ZnTe.[68] A substantial improvement in bandwidth detection and sensitivity may be obtained by using materials with phonon resonance occurring at higher THz frequencies. Among inorganic media with comparable nonlinear optical properties zinc selenide (lowest TO phonon resonance at 6 THz),[11] GaAs (TO phonon resonance at 8 THz), and GaP (TO phonon resonance at 11 THz)[71] are excellent candidates. To verify the performance of electro-optic sampling with GaAs, Vosseburger et al.[72] performed time-resolved experiments of THz radiation detection using bulk GaAs as the electrooptic sampling element. An excitation wavelength of 900 nm was chosen to avoid photoexcitation of carriers by interband absorption in the GaAs. The measured THz radiation pulse had a complex

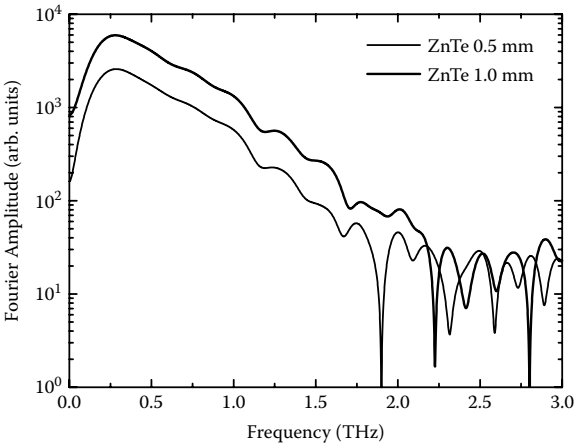

FIGURE 2.7 Fourier amplitudes of the time domain measurements displayed in Figure 2.6. The thinner ZnTe crystal has a slightly larger bandwidth than the thicker ZnTe crystal. The calculated bandwidths of a 0.5-mm and a 1.0-mm ZnTe crystal are 2.86 THz and 2.62 THz, respectively. (Adapted from Selig, H., Elektro-optisches Sampling von Terahertz Pulsen, Hochschulschrift: Hamburg, Universitaet, Fachbereich Physik, Diplomarbeit, 35,2000. With permission.)

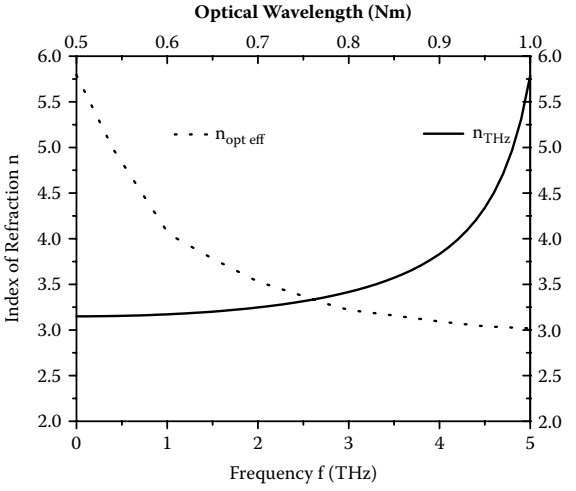

FIGURE 2.8 Index of refraction of ZnTe at optical wavelength ($n_{\text{opt eff}}$) and THz frequencies (n_{THz}). Optical radiation at 760-μm wavelength propagates at the same speed as 2.6 THz-frequency radiation in ZnTe. The effective index of refraction at $\lambda = 780$ μm is $n_{\text{opt eff}} = 3.27$. (Adapted from Selig, H., Elektro-optisches Sampling von Terahertz Pulsen, Hochschulschrift: Hamburg, Universitaet, Fachbereich Physik, Diplomarbeit, 33, 2000. With permission.)

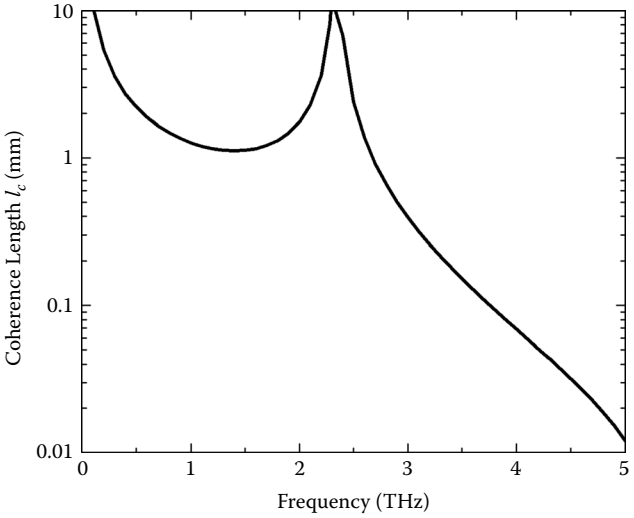

FIGURE 2.9 Calculated coherence length l_c of ZnTe as a function of THz frequency for λ = 780 μm. (Adapted from Selig, H., Elektro-optisches Sampling von Terahertz Pulsen, Hochschulschrift: Hamburg, Universitaet, Fachbereich Physik, Diplomarbeit, 7, 2000. With permission.)

temporal structure and was smaller by a factor of approximately 20 compared with the same pulse measured by a ZnTe crystal. The reduction in amplitude had its origins in the smaller electrooptic coefficient of GaAs than that of ZnTe and poor phase matching of GaAs at 900 mm and 1 THz.

Among zincblende crystals, GaP is an excellent alternative to ZnTe for electrooptic sampling of THz-frequency radiation because of its high-frequency phonon band at 11 THz,[71] the highest available among all zincblende crystals. The electrooptic coefficient of GaP ($r_{41} \approx 0.97$ pm/V[30]), however, is one fourth that of ZnTe. In 1997, Wu and Zhang[73] first demonstrated electrooptic sampling of THz radiation with a GaP crystal. Using a GaAs emitter excited by 50-fs pulses and a 150-μm thick <110> GaP crystal, they demonstrated a bandwidth resolution up to 7 THz. Broadband THz electrooptic sampling with GaP crystals was further developed by Leitenstorfer et al.[74] They carefully evaluated the frequency dependence of the refractive index, the electrooptic coefficient and the response function of the GaP electrooptic THz detector. Using a 13-μm thick crystal and 12-fs titanium–sapphire laser pulses the detected spectral bandwidth of GaP was estimated to be ~70 THz.

One of the recently reported materials used for free-space electrooptic sampling of THz radiation is ZnSe in crystalline and polycrystalline form.[75] Although the electrooptic coefficient of ZnSe ($r_{41} \approx 2$pm/V[75]) is only half of that of ZnTe, the TO phonon resonance frequency (6 THz)[11] is higher than that of ZnTe (5.4 THz),[11] thus promising a higher detection bandwidth potential for the former. The GVM for ZnSe (0.96 pm/V[75]) is comparable to that for ZnTe. Using a 10-fs titanium–sapphire laser pulse to excite a 100-μm GaAs photoconducting antenna and a 0.5-mm, <111>-oriented ZnSe single crystal as detector, a spectral bandwidth of 3 THz was

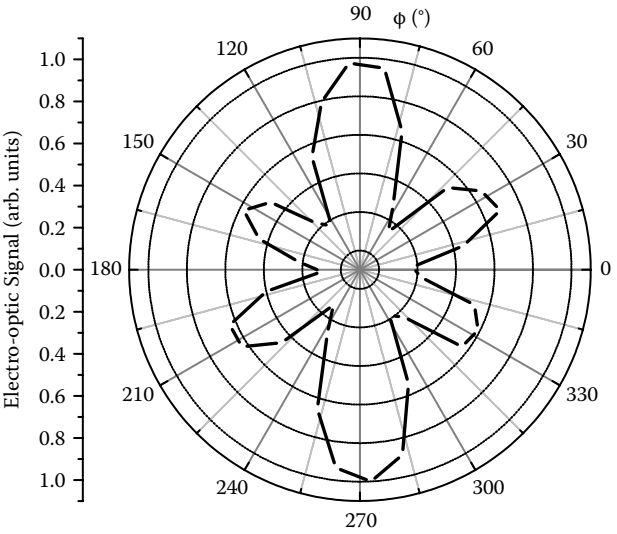

FIGURE 2.10 Measurements of the peak electrooptic signal as a function of the angle Φ between the <001> direction of a <110> ZnTe crystal and the direction of linear polarization of the optical probe beam. The polarization of the THz pulse is perpendicular to the polarization of the optical probe pulse. During the measurements, the orientations of the polarization of the optical and the THz pulses are fixed and the crystal is turned in steps of 10°. An angle Θ = 90° corresponds to the situation in which the polarization of the optical probe beam is parallel to the <001> direction of the ZnTe. Two major maxima at Θ = 90° and Θ = 270° and four minor maxima at Θ = 30°, Θ = 150°, Θ = 210°, and Θ = 330° are observed. The amplitude of the peak THz electric field is estimated to be 5 V/m. (Adapted from Selig, H., Elektro-optisches Sampling von Terahertz Pulsen, Hochschulschrift: Hamburg, Universitaet, Fachbereich Physik, Diplomarbeit, 47, 2000. With permission.)

measured. In this experiment, the bandwidth detected by the ZnSe crystal was limited only by the generation of the THz radiation. It was found that for thicker (1 mm) polycrystalline electrooptic ZnSe samples, the random nature of crystallographic orientations within the interaction length distorted the phase of THz waveform. However, a reduction of the thickness to 0.15 mm minimized the distortion and extended the bandwidth up to 4 THz. Because polycrystalline semiconductors offer practical advantages in terms of ease of fabrication[75] over their single crystal counterparts, the successful application of polycrystalline materials for free-space electrooptic sampling permits the possibility of utilizing non-lattice matched thin film integrated electrooptic detectors of THz radiation.

As discussed previously, the mismatch between THz phase velocity and the group velocity of the optical probe pulse limits the detection bandwidth of zincblende electrooptic crystals such as ZnTe and GaP. However, this limitation can be eliminated by using a novel detection scheme, taking advantage of the type II phase matching in a naturally birefringent crystal such as GaSe.[53,76] The phase matching condition can be satisfied by angle tuning whereby the electrooptic crystal

TABLE 2.4
Properties of Typical Electrooptic Sensor Materials*

Material	Crystal Structure	Point Group	Electrooptic Coefficient (pm/V)	Group Velocity Mismatch (ps/mm)	Surface Orientation	Experimental Detection Bandwidth (THz)†
ZnTe	Zincblende[30]	$\bar{4}3m$[30]	$r_{41} = 3.90$[30]	1.1[68]	110[11]	2.5[11]
GaP	Zincblende[30]	$\bar{4}3m$[30]	$r_{41} = 0.97$[30]	—	110[73]	7[73]
ZnSe	Zincblende[30]	$\bar{4}3m$[30]	$r_{41} = 2.00$[30]	0.96[75]	111[75]	3[75]
LiTaO3	Trigonal[30]	$3m$[30]	$r_{33} = 30.3$[30] $r_{13} = 5.70$	14.1[68]	—	—
GaSe	Hexagonal[53]	$\bar{6}2m$[53]	$r_{22} = 14.4$[76]	0.10[76]	—	120[76]
DAST	—	—	$r_{11} = 160$[68]	1.22[68]	—	6.7[77]
Poled polymers	—	—	—	—	—	33[78]

* A more comprehensive listing may be found in reference 68.

† The bandwidth reported here is subject to experimental conditions and not the absolute bandwidth for a particular emitter/sensor material.

(z-cut GaSe crystal) is tilted by an angle θ_{det} (the phase matching angle) about a horizontal axis perpendicular to the direction of time-delayed probe beam.[76] In the experiments conducted by Kubler and coworkers,[76] a THz radiation pulse was generated by optical rectification of 10-fs titanium–sapphire laser pulses in a 20-μm thick GaSe crystal ($\theta_{em} = 57°$) and detected with a GaSe sensor ($\theta_{det} = 60°$) of thickness 30 μm. $\theta_{det/em} = 0$ signifies normal incidence. The amplitude spectrum of the THz pulse peaked at 33.8 THz and extended from 7 THz to beyond 120 THz. Compared with a 12-μm thick ZnTe crystal that displayed a local minimum at 34 THz under the same excitation, the GaSe spectrum showed a nearly flat response from 10 THz up to 105 THz. The enhanced performance of GaSe crystals over ZnTe crystals is attributed mainly to a greater interaction length because of better phase matching and a larger electrooptic coefficient of GaSe (Table 2.4).

2.4.1.2 Organic Crystals

In the quest for novel materials for electrooptic sampling of THz radiation pulses, organic electrooptic crystals have attracted attention owing to their very high electrooptic coefficients. Han and coworkers[55] first demonstrated the application of the organic ionic salt crystal DAST as a free space electrooptic detector of THz radiation. The electrooptic coefficient for DAST is 160 pm/V at 820 nm[68] and is almost two orders higher than that found in ZnTe (Table 2.4). However, DAST exhibits two confirmed phonon absorption peaks at 1.1 THz and 3.05 THz.[77] Recently, nonlinear optical generation and detection of THz radiation pulses was investigated theoretically and experimentally by Schneider et al.[77] They demonstrated that the THz radiation spectrum generated and detected using DAST crystals extended from 0.4 THz to 6.7 THz, depending on the laser excitation wavelength in the 700-nm

to 1,600-nm wavelength range. Furthermore, they found that the technologically important wavelengths around 1,500 nm are velocity matched to THz frequencies between 1.5 THz and 2.7 THz.

Among other organic materials, poled polymers have been reported to exhibit excellent broadband electrooptic detection capability.[78] These materials demonstrate large electrooptic coefficients,[79] low dispersion between the THz and optical refractive indices,[57,80] ease of fabrication in large area thin films, and easily modifiable chemical structures for better THz and optical properties because of their organic nature. Using poled polymers for free-space electrooptic detection, Nahata and coworkers[78] recently measured an amplitude spectrum up to frequencies of 33 Hz.

2.5 APPLICATION OF ELECTROOPTIC SAMPLING OF THZ ELECTRIC FIELD TRANSIENTS

Nonlinear techniques for the generation and detection of short pulses of THz-frequency radiation have found important applications such as time domain THz spectroscopy and time domain THz imaging.[34] Here, we discuss briefly the application of electrooptic sampling of THz radiation pulses to longitudinal electron bunch length measurements.

The electrooptic detection of the local nonradiative electric field that travels with a relativistic electron bunch has recently emerged as a powerful new technique for subpicosecond electron bunch length measurements.[81–84] The method makes use of the fact that the local electric field of a highly relativistic electron bunch that moves in a straight line is almost entirely concentrated perpendicular to its direction of motion. Consequently, the Pockels' effect induced by the electric field of the passing electron bunch can be used to produce birefringence in an electrooptic crystal placed in the vicinity of the beam. Specifically, the birefringence induced by a single electron bunch is measured by monitoring the change of polarization of the wavelength components of a chirped, synchronized titanium–sapphire laser pulse. When the electric field of an electron bunch and the chirped optical pulse copropagate in the electrooptic crystal, the polarizations of the various wavelength components of the chirped pulse that passes through the crystal are rotated by different amounts that correspond to different portions of the local electric field. The direction and degree of rotation are proportional to the amplitude and the phase of the electric field. Thus the time profile of the local electric field of the electron bunch is linearly encoded to the wavelength spectrum of the optical probe beam. An analyzer converts the modulation of the polarization of the chirped optical pulse into an amplitude modulation of its spectrum. The time profile of the electric field of the electron bunch is measured as the difference of the spectrum with and without a copropagating electron bunch. The width of the temporal profile corresponds directly to the electron bunch length, and the shape of the temporal profile is proportional to the longitudinal electron distribution within the electron bunch. The length and the shape of individual electron bunches are determined by measuring the spectra of single chirped laser pulses with an optical multichannel analyzer equipped with a nanosecond shutter. The method allows direct in situ electron bunch diagnostics with a high signal-to-noise ratio and subpicosecond time resolution.

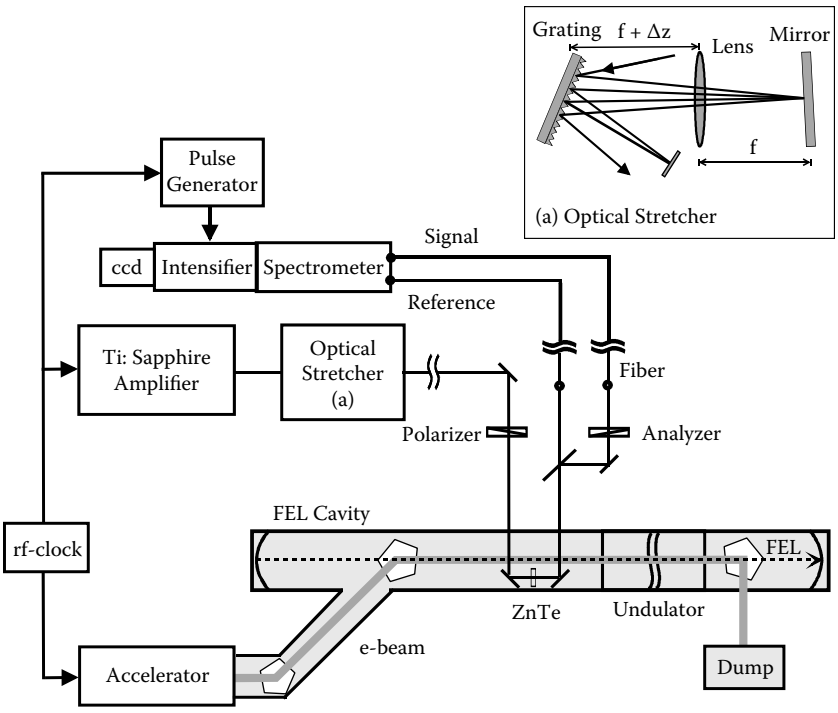

FIGURE 2.11 Experimental setup for electron bunch length measurements by electrooptic sampling with chirped optical pulses. The electron bunch length is measured by using a ZnTe crystal placed inside the vacuum pipe at the entrance of the undulator. The femtosecond near infrared laser repetition rate is synchronized with the repetition rate of the electron bunches. The inset (a) exhibits a two-dimensional optical stretcher for laser pulse chirping. (Adapted figure with permission from I. Wilke, A. M. McLeod, W. A. Gillespie, G. Berden, G. M. H. Knippels, A. F. G. van der Meer, *Phys. Rev. Lett.* 88, 124801-1 (2002). Copyright 2002 by the American Physical Society.)

The experimental arrangements for the electrooptic electron bunch length measurements are schematically illustrated in Figure 2.11. The electron bunch source is the radiofrequency linear accelerator at the FELIX free electron laser facility in the Netherlands.[85] The electron beam energy of FELIX was set at 46 MeV, and its charge per bunch at around 200 pC. The micropulse repetition rate was 25 MHz, and the macropulse duration was around 8 μ with a repetition rate of 5 Hz. A titanium–sapphire amplifier, producing 30-fs FWHM pulses at 800 nm with a repetition rate of 1 kHz, was used as a probe beam. The 30-fs optical laser pulses are chirped to pulses of up to 20 ps (FWHM) duration with an optical stretcher which consists of a grating, a lens, and a plane mirror.[86] The duration of the chirped pulses has been measured with an optical autocorrelator based on second harmonic generation in a BBO crystal.

The electron bunch length is measured inside the accelerator beam pipe at the entrance of the undulator. A 0.5-mm thick <110> ZnTe crystal is used as an

electrooptic sensor and is placed with its 4 × 4 mm^2 front face perpendicular to the propagation direction of the electron beam. The incoming chirped laser beam is linearly polarized. The outgoing chirped beam is split into a signal beam and a reference beam used to monitor possible laser power fluctuations. The signal beam passes through an analyzer (a second polarizer), which is crossed with respect to the first polarizer. Subsequently, the spectra of the chirped laser pulses are dispersed with a grating spectrometer and the line spectra are focused onto a charge-coupled device (CCD) camera. The CCD camera is equipped with an intensifier, which acts as a nanosecond shutter with a gate width of 100 ns. Single-shot measurements are performed by actively synchronizing the titanium–sapphire amplifier[87] with both the repetition rate of the electron beam and the gate of the CCD camera, and therefore recording only the spectrum of one chirped laser pulse at a time. The temporal overlap between the electron bunch and chirped laser pulse is controlled by an electronic delay.

Figure 2.12a shows measurements of the chirped laser pulse spectra with and without a copropagating electron bunch. The signal spectra are labeled by S and S′. The crossed polarizers exhibit a finite transmission of 1.7% if the electron bunch does not overlap with the chirped laser pulse. This is attributed to a small intrinsic stress birefringence of the ZnTe. The transmission of the crossed polarizers changes significantly when the electron bunch and the laser pulse copropagate: in these circumstances, a large peak, which corresponds to a strong enhancement of the transmission, is observed in the center of the spectrum. The strong change of the spectrum is attributed to the wave length-dependent change in polarization of the chirped laser pulse because of the electric field of the electron bunch. The length and shape of the electron bunch is obtained by subtracting the spectrum without copropagating electron bunch, which has been corrected for laser power fluctuations by multiplication with the ratio of the reference spectra R/R′ from the spectrum with copropagating electron bunch. This difference S−(S′R/R′) is corrected for the wavelength-dependent variations in intensity in the spectrum by dividing by the spectrum S′R/R′. The pixels are converted to time by measuring the length of the chirp τ, the spectral resolution of the spectrometer and CCD setup, $\Delta\lambda/pixel$, and the bandwidth of the chirped laser pulses $\Delta\lambda_{bw}$. Then, the time interval per pixel is given by $(\Delta t/pixel) = (\Delta\lambda/pixel)/(\tau/\Delta\lambda_{bw})$. For the spectra of Figure 2.12a, the chirp was 4.48 ps FWHM, which results in an electron bunch measurement as displayed in Figure 2.12b. The width of the electron bunch is (1.72 ± 0.05) ps FWHM. The signal-to-noise ratio depends on the position in the spectrum; in the center of the spectrum, it is better than 200:1. The measured width and shape of a single electron bunch agree very well with the electron bunch measurements averaged over more than 8,000 electron bunches[88] and CTR measurements.[89]

Linear accelerators used as drivers for new femtosecond x-ray free-electron lasers or employed in new teraelectron volt linear electronpositron colliders for high-energy physics, require dense, relativistic electron bunches with bunch lengths shorter than a picosecond. Precise measurements of the electron bunch length and its longitudinal charge distribution are important to monitor the preservation of the beam quality, whereas the electron bunch train travels through the beam pipe, as well as to tune and to operate a linear collider or a FEL.

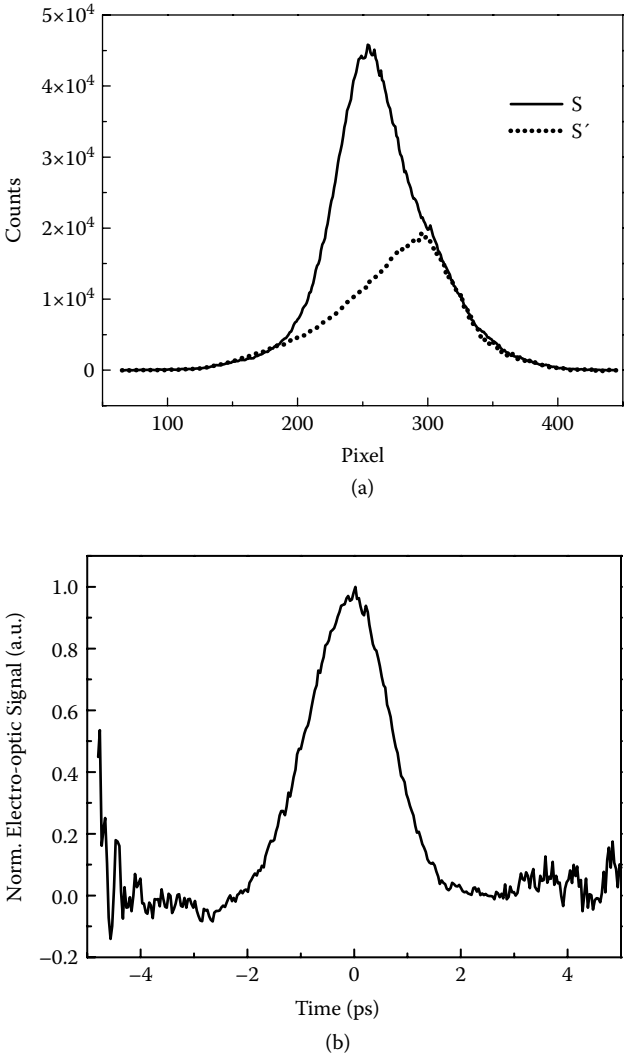

FIGURE 2.12 Fig. 2.12 (a) Measurements of the chirped laser pulse spectra with(s) and without (s′) a copropagating electron bunch. (b) single shot electron bunch length measurements. The width of the electron bunch is (1.72 ± 0.05) ps FWHM.

REFERENCES

1. Mittleman, D., Ed., *Sensing with terahertz radiation*, Springer Optical Science 85. Berlin: Springer, 2003.
2. Nuss, M. C., and Orenstein, J., Terahertz time-domain spectroscopy, in *Millimeter and sub-millimeter-wave spectroscopy of solids*, Grüner, G., ed., Topics in Applied Physics 74. Berlin: Springer, 1998.

3. Brucherseifer, M., et al., Label free probing of binding state of DNA by time-domain terahertz sensing, *Appl. Phys. Lett.*, 77, 4049, 2000.
4. Kaindl, R. L., et al., Ultrafast terahertz probes of transient conducting and insulating phases in an electron-hole gas, *Nature*, 423, 73, 2003.
5. Corson, J., et al., Vanishing of phase coherence in underdoped $Bi_2Sr_2CaCu_2O_{8+\delta}$ *Nature*, 398, 221, 1999.
6. Karpowicz, N., et al., Compact continuous-wave terahertz system for inspection applications, *Appl. Phys. Lett.*, 86, 54105, 2005.
7. Wallace, V. P. et al., Terahertz pulsed imaging and spectroscopy for biomedical and pharmaceutical applications, *Faraday Discuss.*, 126, 255, 2004.
8. Yang, K. H., Richards, P. L., and Shen, Y. R., Generation of far-infrared radiation by picosecond light pulses in $LiNbO_3$, *Appl. Phys. Lett.*, 19, 320, 1971.
9. Zhang, X. C., Jin, Y., and Ma, X. F., Coherent measurement of terahertz optical rectification from electrooptic crystals, *Appl. Phys. Lett.*, 61, 2764, 1992.
10. Hu, B. B., et al., Free-space radiation from electrooptic crystals, *Appl. Phys. Lett.*, 56, 506, 1990.
11. Nahata, A., Weling, A. S., and Heinz, T. F., A wideband coherent terahertz spectroscopy system using optical rectification and electrooptic sampling, *Appl. Phys. Lett.*, 69, 2321, 1996.
12. Han, P. Y., and Zhang, X. C., Free-space coherent broadband terahertz time-domain spectroscopy, *Meas. Sci. Technol.*, 12, 2001, 1747.
13. Rice, A., et al., Terahertz optical rectification from <110> zinc-blende crystals, *Appl. Phys. Lett.*, 64, 1324, 1994.
14. Nagai, M. et al., Generation and detection of terahertz radiation by electrooptical process in GaAs using 1.56 μm fiber laser pulses, *Appl. Phys. Lett.*, 85, 3974, 2004.
15. Huber, R., et al., Generation and field resolved detection of femtosecond electromagnetic pulses tunable up to 41 THz, *Appl. Phys. Lett.*, 76, 3191, 2000
16. Shi, W. et al., Efficient, tunable and coherent 0.18–5.27-THz source based on GaSe crystal, *Opt. Lett.*, 27, 1454, 2002.
17. Xie, X., Xu, J., and Zhang, X.C., Terahertz wave generation and detection from a CdTe crystal characterized by different excitation wavelengths, *Opt. Lett.*, 31, 978, 2006.
18. Liu, K. et al., Study of ZnCdTe crystals as THz wave emitters and detectors, *Appl. Phys. Lett.*, 81, 4115, 2002.
19. Zhang, X.C. et al., Terahertz optical rectification from a nonlinear organic crystal, *Appl. Phys. Lett.*, 61, 3080, 1992.
20. Kadlec, F., Kuzel, P., and Coutaz J.L., Optical rectification at metal surfaces, *Opt. Lett.*, 29, 2674, 2004.
21. Kadlec, F., Kuzel, P., and Coutaz J.L., Study of terahertz radiation generated by optical rectification on thin gold films, *Opt. Lett.*, 30, 1402, 2005.
22. Bass, M., et al., Optical rectification, *Phys. Rev. Lett.*, 9, 446, 1962.
23. Zernike, F., Jr., and Berman, P. R., Generation of far infrared as a difference frequency, *Phys. Rev. Lett.*, 15, 999, 1965.
24. Pockels, F., Lehrbuch der Kristalloptik, Bibliotheca Mathematica Teubneriana. Leipzig: Band 39, 1906.
25. Harris, S. E., McMurtry, B. J., and Siegman, A. E., Modulation and direct demodulation of coherent and incoherent light at microwave frequency, *Appl. Phys. Lett.*, 1, 37, 1962.
26. Valdmanis, J. A., Mourou, G., and Gabel, C. W., Picosecond electrooptic sampling system, *Appl. Phys. Lett.*, 41, 211, 1982.
27. Wu, Q., and Zhang, X. C., Free-space electrooptic sampling of terahertz beams, *Appl. Phys. Lett.*, 67, 3523, 1995.

28. Jepsen, P. U., et al., Detection of THz pulses by phase retardation in lithium tantalate, *Phys. Rev.* E, 53, 3052, 1996.
29. Nahata, A., et al., Coherent detection of freely propagating terahertz radiation by electrooptic sampling, *Appl. Phys. Lett.*, 68, 150, 1996.
30. Yariv, A., *Modulation of optical radiation, in quantum electronics,* 3rd ed., Hoboken, NJ. John Wiley & Sons, 1988.
31. Armstrong, J. A., et al., Interactions between light waves in a non-linear dielectric, *Phys. Rev.*, 127, 1918, 1962.
32. Bonvalet, A. and Joffre, M., Terahertz femtosecond pulses, in *Femtosecond laser pulses: principles and experiments*, Rullière, C., ed., Berlin: Springer, 1998.
33. Shen, J., Nahata, A., and Heinz, T. F., Terahertz time-domain spectroscopy based on nonlinear optics, *J. Nonlinear Opt. Phys.*, 11, 31, 2002.
34. Jiang, Z., and Zhang X. C., Free space electrooptic techniques, in *Sensing with terahertz radiation*, Optical Science 85, Mittleman, D., ed., Berlin: Springer, 2003, 155.
35. Franken, P. A., and Ward, J. F., Optical harmonics and nonlinear phenomena, *Rev. Mod. Phys.*, 35, 23, 1963.
36. Hirlimann, C., Further methods for the generation of ultrashort optical pulses, in *Femtosecond laser pulses: principles and experiments*, Rullière, C., ed., Berlin: Springer, 1998.
37. Planken, P. C. M., et al., Measurement and calculation of the orientation dependence of terahertz pulse detection in ZnTe, *J. Opt. Soc. Am. B.*, 18, 313, 2001.
38. Zhang, X. C. et al., Generation of femtosecond electromagnetic pulses from semiconductor surfaces, *Appl. Phys. Lett.*, 56, 1011, 1990.
39. Greene, B. I., et al., Interferometric characterization of 160 fs far-infrared light pulses, *Appl. Phys. Lett.*, 59, 893, 1991.
40. Zhang, X. C., and Auston, D. H., Optoelectronic measurement of semiconductor surfaces and interfaces with femtosecond optics, *J. Appl. Phys.*, 71, 326, 1992.
41. Jin, Y. H., and Zhang, X. C., Terahertz optical rectification, *J. Nonlinear Opt. Phys.*, 4, 459, 1995.
42. Chuang, S. L. et al., Optical rectification at semiconductor surfaces, *Phys. Rev. Lett.*, 68, 102, 1992.
43. Greene, B. I., et al., Far-infrared light generation at semiconductor surfaces and its spectroscopic applications, *IEEE J. Quantum Electron*, 28, 2302, 1992.
44. Reid, M., Cravetchi, I. V., and Fedosejevs, R., Terahertz radiation and second harmonic generation from InAs: bulk versus surface electric field induced contributions, *Phys. Rev. B.*, 72, 035201-1, 2005.
45. Chang, G., et al., Power scalable compact THz system based on an ultrafast Yb-doped fiber amplifier, *Opt. Express*, 14, 7909, 2006.
46. Gu, P., et al., Study of THz radiation from InAs and InSb, *J. Appl. Phys.*, 91, 5533, 2002.
47. Reid, M., and Fedosejevs, R., Terahertz emission from (100) InAs surface at high excitation fluences, *Appl. Phys. Lett.*, 86, 011906-1, 2005.
48. Lewis, R. A., et al., Terahertz generation in InAs, *Physica B*, 376, 618, 2006.
49. Adomavicius, R., et al., Terahertz emission from p-InAs due to instantaneous polarization, *Appl. Phys. Lett.*, 85, 2463, 2004.
50. Reid, M. and Fedosejevs, R., Terahertz emission from surface optical rectification in n-InAs, *Proc. of SPIE*, 5577, 659, 2004.
51. Ching, W. Y., and Huang, M. Z., Calculation of optical excitations in cubic semiconductors. III. Third-harmonic generation, *Phys. Rev. B*, 47, 9479, 1993.
52. Kang, H. S., et al., *Technical digest of Pacific Rim conference on lasers and electro-optics*. New York: IEEE, 1107, 1999.

53. Liu, K., Xu, J., and Zhang, X. C., GaSe crystals for broadband terahertz wave detection, *Appl. Phys. Lett.*, 85, 863, 2004.
54. Auston, D. H. and Cheung, K. P, Coherent time domain far-infrared spectroscopy, *J. Opt. Soc. Am. B*, 2, 606, 1985.
55. Han, P. Y., et al., Use of organic crystal DAST for terahertz beam applications, *Opt. Lett.*, 25, 675, 2000.
56. Schneider, A., and Gunter, P., Spectrum of terahertz pulses from organic DAST crystals, *Ferroelectrics*, 318, 83, 2005.
57. Nahata, A., et al., Generation of terahertz radiation from a poled polymer, *Appl. Phys. Lett.*, 67, 1358, 1995.
58. Khanarian, G., Mortazavi, M. A., and East, A. J., Phase matched second-harmonic generation from free standing periodically stacked polymer films, *Appl. Phys. Lett.*, 63, 1462, 1993.
59. Hashimoto, H., et al., Characteristics of terahertz radiation form single crystals of N-substituted 2-methyl-4-nitroaniline, *J. Phys.: Condens. Matter*, 13, L529, 2001.
60. Kuroyanagi, K., et al., All organic terahertz electromagnetic wave emission and detection using highly purified N-benzyl-2-methyl-4-nitroaniline crystals, *Jpn. J. Appl. Phys.*, 45, 4068, 2006.
61. Carey, J. J., et al., Terahertz pulse generation in an organic crystal by optical rectification and resonant excitation of molecular charge transfer, *Appl. Phys. Lett.*, 81, 4335, 2002.
62. Bailey, R. T., et al., The linear optical properties of the organic molecular crystal (+) 2-(α-methylbenzylamino)-5-nitropyridine (MBA-NP), *Mol. Cryst. Liq. Cryst.*, 231, 223, 1993.
63. Bailey, R. T., et al., Linear electrooptic dispersion in (-)-2-(α-methylbenzylamino)-5-nitropyridine single crystals, *J. Appl. Phys.*, 75, 489, 1994.
64. Loffler, T., et al., Comparative performance of terahertz emitters in amplifier-laser-based systems, *Semicond. Sci. Technol.*, 20, S134, 2005.
65. Siders, J. L. W., et al., Terahertz emission from $YBa_2Cu_3O_{7-\delta}$ thin films via bulk electric-quadrupole-magnetic-dipole optical rectification, *Phys. Rev. B*, 61, 13633, 2000.
66. Hilton, D. J., et al., Terahertz emission via ultrashort-pulse excitation of magnetic metal films, *Opt. Lett.*, 29, 1805, 2004.
67. Mikheev, G. M., et al., Giant optical rectification effect in nanocarbon films, *Appl. Phys. Lett.*, 84, 4854, 2004.
68. Wu, Q., and Zhang, X. C., Ultrafast electrooptic field sensors, *Appl. Phys. Lett.*, 68, 1604, 1996.
69. Wu, Q., and Zhang, X. C., Electrooptic sampling of freely propagating terahertz fields, *Opt. Quantum Electron.*, 28, 945, 1996.
70. Han, P. Y., and Zhang, X. C., Coherent, broadband midinfrared terahertz beam sensors, *Appl. Phys. Lett.*, 73, 3049, 1998.
71. Handbook series on semiconductor parameters, Levinstein, M., Rumyantsev, S., and Shur, eds., London: World Scientific, 1996, 1999. Available online at http://www.ioffe.rssi.ru/SVA/NSM/Semicond/.
72. Vosseburger, M., et al., Propagation effects in electrooptic sampling of THz pulses in GaAs., *Appl. Opt.*, 37, 3368, 1998.
73. Wu, Q., and Zhang, X. C., Seven terahertz broadband GaP electrooptic sensor, *Appl. Phys. Lett.*, 70, 1784, 1997.
74. Leitenstorfer, A., et al., Detectors and sources for ultrabroadband electrooptic sampling: experiment and theory, *Appl. Phys. Lett.*, 74, 1516, 1999.

75. Holzman, J. F., et al., Free-space detection of terahertz radiation using crystalline and polycrystalline ZnSe electrooptic sensors, *Appl. Phys. Lett.*, 81, 2294, 2002.
76. Kubler, C., Huber, R., and Leitenstorfer, A., Ultrabroadband terahertz pulses: generation and field-resolved detection, *Semicond. Sci. Technol.*, 20, S128, 2005.
77. Schneider, A., et al., Generation of terahertz pulses through optical rectification in organic DAST crystals: theory and experiment, *J. Opt. Soc. Am. B*, 23, 1822, 2006.
78. Nahata, A., and Cao, H., Broadband phase-matched generation and detection of terahertz radiation, *Proc. SPIE*, 5411, 151, 2004.
79. Shi, Y. Q., et al, Electrooptic polymer modulators with 0.8 V half-wave voltage, *Appl. Phys. Lett.*, 77, 1, 2000.
80. Sinyukov, A. M., and Hayden, L. M., Generation and detection of terahertz radiation with multilayered electrooptic polymer films, *Opt. Lett.*, 27, 55, 2002.
81. Van Tilborg, J., et al., Terahertz radiation as a bunch diagnostic for laser-wakefield-accelerated electron bunches, *Phys. Plasmas*, 13, 56704–1, 2006.
82. Berden, G., et al., Electrooptic technique with improved time resolution for real time, nondestructive, single shot measurements of femtosecond electron bunch profiles, *Phys. Rev. Lett.*, 93, 114802/1, 2004.
83. Wilke, I., Single-shot electron-beam bunch length measurements, *Phys. Rev. Lett.*, 88, 124801/1, 2002.
84. Tsang, T., et al., Electrooptical measurements of picosecond bunch length if 45 MeV electron beam, *J. Appl. Phys.*, 89, 4921, 2001.
85. Oepts, D., van der Meer, A. F. G., van Amersfoort, P. W., The free-electron-laser user facility FELIX, *Infrared Phys. Techn.*, 36, 297, 1995.
86. Knippels, G. M. H., et al., Generation of frequency-chirped pulses in the far-infrared by means of a sub-picosecond free-electron laser and an external pulse shape, *Opt. Commun.*, 118, 546, 1995.
87. Knippels, G. M. H., et al., Two-color facility based on a broadly tunable infrared free-electron laser and a subpicosecond-synchronized 10-fs Ti:sapphire laser, *Opt. Lett.*, 23, 1754, 1998.
88. Yan, X., et al., Subpicosecond electrooptic measurement of relativistic electron pulses, *Phys. Rev. Lett.*, 85, 3404, 2000.
89. Ding, M., Weits, H. H., and Oepts, D., Coherent transition radiation diagnostic for electron bunch shape measurement at FELIX**,** *Nucl. Instrum. Meth. A*, 393, 504, 1997.